ACS OMEGA

http://pubs.acs.org/journal/acsodf

Article

Mono- and Multicomponent Biosorption of Caffeine and Salicylic Acid onto Processed Cape Gooseberry Husk Agri-Food Waste

Jehan Abdel Salam,[‖] Amina A. Saleh,[‖] Toqa Taha El Nenaiey, Hu Yang, Tamer Shoeib,* and Mayyada M. H. El-Sayed*

Cite This: *ACS Omega* 2023, 8, 20697−20707

Read Online

ACCESS | Metrics & More | Article Recommendations | Supporting Information

ABSTRACT: There is an increasing need to find cost-effective and sustainable solutions for treating wastewater from contaminants of emerging concern (CECs). In this regard, cape gooseberry husk—typically an agri-food waste—is investigated for the first time as a potential biosorbent for the removal of model pharmaceutical contaminants of caffeine (CA) and salicylic acid (SA) from water. Three different preparations of husks were investigated and characterized using Fourier transform infrared spectroscopy, scanning electron microscopy, Brunauer−Emmett−Teller analysis, zeta potential, and point of zero charge measurements. The activation of the husk led to an increase in the surface area, pore volume, average pore size, and adsorption favorability. The single-component adsorption of SA and CA onto the three husks was investigated at different initial concentrations and pH values to determine the optimal operating conditions. The maximal removal efficiencies of SA and CA reached up to 85 and 63%, respectively, for the optimal husk which also offers a less energy-intensive option in its activation. This husk also exhibited high rates of adsorption that exceeded other husk preparations by up to four times. It was proposed that CA interacts electrostatically with the husk, while SA binds through weak physical interactions (e.g., van der Waals and H-bonding). In binary systems, CA adsorption was highly favored over SA adsorption, owing to its electrostatic interactions. The selectivity coefficients α_{SA}^{CA} varied with initial concentration and ranged between 61 and 627. The regeneration of husk was also successful resulting in its re-use for up to four full consecutive cycles, further demonstrating the efficiency of cape gooseberry husk use in wastewater treatment.

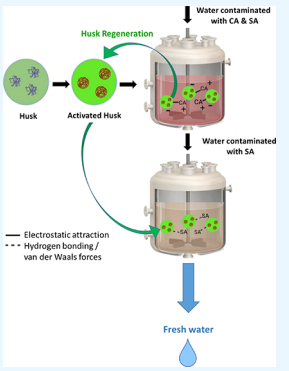

1. INTRODUCTION

Contaminants of emerging concern (CECs) are of an increasing environmental and legislative concern worldwide, since their persistence in water bodies results in disruptions to the ecosystem and consequent hazards to human health.[1−5] Adverse effects include aquatic toxicity, development of pathogenic bacteria resistance, human hormonal disturbance, and genotoxicity.[6] Over the last decades, the production and the use of medications have tremendously increased; around 3000 different compounds are being utilized in the pharmaceutical industry as ingredients, and, as a result, hundreds of tons are annually produced.[7] Unfortunately, massive amounts of these contaminants are discharged into surface water bodies.

Salicylic acid (SA) and caffeine (CA) are among the most widespread pharmaceuticals and can become harmful to humans, if present beyond their threshold concentration levels.[8] SA is mainly utilized as an analgesic and antipyretic drug, in addition to its action in preventing platelet aggregation.[9] It is also an important ingredient in cosmetic products because of its antiseptic, disinfecting, and keratinolytic properties.[10] In spite of its importance, high concentrations of SA can be toxic, causing headache, nausea, and disruption to the kidney and liver functions.[11] As for CA which is considered a tracer for human pollution being almost entirely human-related,[2] it is used in the beverage industry as a stimulant that belongs to the group of xanthines. In the pharmaceutical industry, CA is used in many painkillers and other drugs to counteract the effect of drowsiness, as well as a vasodilator and a diuretic.[12] Too much CA would however cause sleep deprivation, risk of cardiovascular diseases, fertility rate reduction, and an increasing probability of miscarriages.[13]

There are several physical, chemical, and biological processes employed to treat the wastewater effluents before they are released into the environment, such as membrane filtration and advanced oxidation processes.[13] These conventional techniques still suffer from technical limitations as well as environmental and economic disadvantages. Biosorption proposes an alternative technique for wastewater treatment, which is potentially eco-friendly and cost-effective since the utilized adsorbents are derived from a natural biobased origin.[14−17] Several agricultural wastes have been successfully used for treating CECs such as rice husk, green tomato husk,

Received: February 24, 2023
Accepted: May 16, 2023
Published: May 30, 2023

coconut husk, and fruit peels.[8,14,18,19] The green tomato and gooseberries are closely related since they belong to the same genus (Physalis). Nevertheless, to the best of our knowledge, no biosorption studies have been conducted on cape gooseberry (*Physalis peruviana*) husk to date. Cape gooseberry, as a backyard fruit, is drawing a lot of attention and becoming more important over the last few years because of its fast-growing nature, productivity, adaptability to different soil conditions, and high nutritional values.[20,21] It is also commonly produced from domestic wastes or effluents of food and beverage industries where the fruit is used to make puree or for jam production.[20]

The aim of this work is to examine the possibility of using cape gooseberry husk as a novel biosorbent for the efficient removal of different CECs such as CA and SA from wastewater. Three preparations of husks (untreated husk and two chemically activated husks) are characterized to determine their chemical structure, composition, textural, and morphological properties. The adsorption of each of SA and CA onto these husks is then investigated in single-component systems to determine the optimum operating conditions. The equilibrium, kinetics, and mechanisms of adsorption are also studied. Based on the adsorption performance, one among the three husks is selected as being optimal. The simultaneous adsorption of SA and CA onto the selected husk is subsequently investigated, along with desorption and regeneration of the husk. This environmentally friendly, and cost-effective process could be integrated in wastewater treatment plants as an add-on polishing process or as an alternative to existing tertiary processes, in addition to its extension to other types of CECs.

2. EXPERIMENTAL METHODS

2.1. Preparation and Treatment of the Husk. Cape gooseberry husk (*Physalis peruviana*) waste was collected from El Beheira Governorate (Egypt) with no required permissions for collection, and rotten husk was excluded. A voucher specimen of the husk collected was identified and deposited in the public herbarium collection at the American University in Cairo. The stem of the husk was removed manually, and then the husk was washed three times each with tap water followed by distilled water. The husk was then dried in an oven (HERAtherm, Thermo Scientific) at 60 °C for 2 h and ground in a blender, and then sieved using 2 mm and 630 μm sieves. Particle sizes smaller than 630 μm and bigger than 2 mm were discarded to ensure consistent subsequent surface treatment.

The size selected ground husk was treated with a 0.2% (v/v) formaldehyde (40% w/v, CARLO ERBA Reagents, France) solution to bleach its color and remove the pigments, to avoid adsorption interference. The husk was left in this solution for 24 h, at pH 4.67 and 25 ± 2 °C. The husk was then washed with distilled water followed by deionized (DI) water (pH = 5.46) until the pH of the filtrate was close to that of DI water (pH = 5.40). Finally, the husk was dried in the oven for 2 h at 60 °C, and samples were stored in falcon tubes in the fridge at 4 °C. The treated husk will be referred to as un-activated husk and denoted by, 'H' throughout the text.

For the activation of the husk, orthophosphoric acid (85.5% v/v) (Brand Chemicals, Egypt) was used, due to its strong oxidizing power along with its minimal environmental hazards in comparison to other acids.[22] The husk was left in H_3PO_4 solution for 24 h, with a ratio of 1:10 (w/v, g/mL) husk to acid. The 120 g sample of the husk was washed with distilled and DI water until the pH of the filtrate was close (18 MΩ cm) to that of the DI water. To study the effect of temperature on the characteristics of the husk and its adsorption performance, different husk samples were treated with H_3PO_4 and heated at either of 350 or 500 °C in an oven for 2 h to produce the activated husks of H350 and H500, respectively. The activated husks were also stored in different falcon tubes in a fridge at 4 °C.

2.2. Preparation of Single and Binary CA and SA Solutions. SA (Oxford, India, 98%) was used to prepare serial dilutions of the following concentrations: 18, 35, 70, 105, 140, 175, 210, 262, 280, and 350 mg/L (ppm). Absorbances of these solutions were measured at 295−298 nm with a UV-spectrophotometer type UV-1650 PC, SHIMADZU, and a calibration curve of SA was constructed to convert the absorbance to concentration.

Pure CA anhydrous (Loba Chemie, India, 98%, HPLC-grade) was used to prepare the different CA solutions. Briefly, 0.389 g of pure CA was diluted in DI water up to 1 L. Serial dilution was performed from the stock solution to obtain 1, 10, 27, 82, 172, 255, and 398 mg/L (ppm). Chromatographic analysis for these solutions was performed on an HPLC (Waters LC 2695-PDA Detector) with a reversed-phase C18 column (Mediterranea 250 × 4.6 mm and a particle size of 5 μm). The mobile phase was acetonitrile and water (60:40 v/v), containing 0.1% by volume phosphoric acid, with a flow rate of 1.0 mL/min. A UV wavelength of 275 nm was used for detection using a Waters 996 photodiode array detector. A calibration curve for CA was constructed.

Binary solutions of 40, 60, 80, 100, and 200 mg/L in both CA and SA at a ratio of 1:1 were prepared. Chromatographic analysis followed the same method adopted for the analysis of CA.

2.3. Characterization of the Husks. *2.3.1. Determination of the Point of Zero Charge (PZC).* For all three preparations of husks, the PZC was determined. The pH of the solutions was adjusted using a 1 M HCl (Assay 37%, Honeywell, Germany) solution or 0.1 M NaOH (Chem-Lab, Belgium) solution. Six different SA solutions, 70 mg/L each, were prepared at pH values of 2, 4, 6, 8,10, and 12. A mass of 0.1 g of each husk was added to 10 mL of each of the solutions. The samples were kept in a shaking water bath (SHA-C water bath shaker, China) for 8 h to ensure complete adsorption, and the final pH was recorded.

2.3.2. Zeta Potential Measurements. A mass of 50 mg of each husk preparation was dispersed in 2 mL of DI water. The pH of each solution was adjusted to 3, 5, 6.2, 8, and 10 using 0.1 M NaOH or 1 M HCl. The samples were introduced into a Zetasizer Nano ZS, Malvern UK. The zeta potential was measured using laser Doppler micro-electrophoresis, while the velocity of the particles was measured using a M3-PALS (Phase analysis Light Scattering).

2.3.3. FTIR Analysis. The FTIR spectra of the husks were determined before and after adsorption to identify the different functional groups, using a Thermos Scientific Nicolet 380 FT-IR spectrometer in the spectral range from 7800 to 350 cm^{-1}, and applying the KBr disc method.

2.3.4. SEM Imaging. Images of the surfaces of the three husk types were taken at magnifications of 25×, 55×, 1000×, 10k×, and 20k× using scanning electron microscopy (SEM, SUPRA 55), at an aperture size of 10 mm and width of 3.5 mm. The husks were coated with gold, using HUMMER 8.0, sputtered at 15 mA for 3 min.

https://doi.org/10.1021/acsomega.3c01254
ACS Omega 2023, 8, 20697−20707

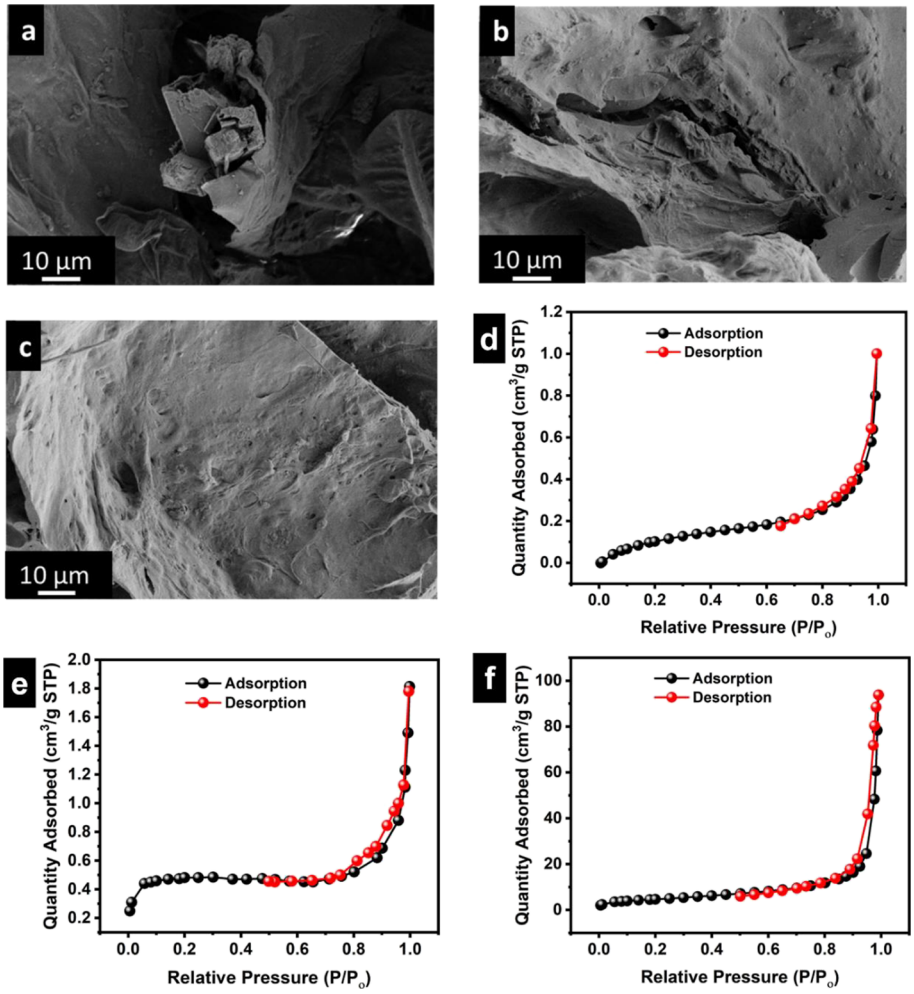

Figure 1. SEM images of (a) un-activated husk H (b) H350, and (c) H500; and BET isotherms for (d) H, (e) H350, and (f) H500. All SEM images are taken at a magnification of 1000×.

2.3.5. Brunauer–Emmett–Teller (BET) Analysis. The surface area and porosity of the husks were determined by nitrogen adsorption at 73 K in an ASAP 2020-Micrometrics equipment. The samples were heated prior to analysis to ensure complete degassing. H, H350, and H500 were heated at 75, 120, and 150 °C, respectively. Pore volumes were estimated using the Barrett–Joyner–Halenda (BJH) model.

2.4. Biosorption Studies. *2.4.1. Effect of pH.* Initial screening experiments were conducted using the three employed husks (H, H350, and H500) to determine the optimal pH for the single-component biosorption of SA or CA. This is the pH corresponding to the highest percent removal achieved within the closest proximity to the neutral pH conditions favored for operational reasons. A volume of 15 mL of either 70 mg/L SA solution or 260 mg/L of CA was added to 0.1 g of each husk, while the pH was adjusted using 0.1 M NaOH or 1 M HCl. The solutions were left at room temperature in a shaking water bath for 8 h. Afterward, the solutions were filtered using a filter paper (Whatman, 8 μm) and the absorbance of the filtrate was measured. For SA, the absorbance was determined using the UV-spectrophotometer (UV-1650 PC, SHIMADZU at a wavelength of 295–298 nm), while an HPLC (Waters LC 2695- PDA Detector) was used for analyzing the CA filtrates at a wavelength of 275 nm. This experiment monitored the effect of pH on the % removal and the equilibrium adsorption capacity (q_e) of H, H350, and H500 for SA and CA.

2.4.2. Effect of Initial Concentration. In this set of experiments, a mass of 0.1 g of husk (H, H350, or H500) was added to 15 mL of each of SA (18–350 mg/L) and CA (10–398 mg/L) solutions. Each mixture was then left shaking in a water bath at room temperature (27 ± 2 °C) and pH 6.5 ± 0.2 for 8 h. The mixtures were then filtered, and the absorbances of the filtrates were measured, following the same methodology described in the previous subsection. The corresponding concentrations of the solutions were calculated using constructed calibration curves. Values of q_e and removal percentage were calculated using eqs S1[23] and S2[24] as shown in the supplementary materials, respectively. For the binary system, only H350 was tested.

2.4.3. Kinetic Modeling of Biosorption. The kinetics of SA and CA adsorption onto H, H350, and H500 in single component systems were studied at different time intervals using the optimal initial concentration of 280 mg/L for SA and 82 mg/L for CA. These two concentrations were chosen based on the removal efficiencies obtained in the biosorption experiments. The biosorption kinetic profiles of SA and CA onto the husks were obtained experimentally and plotted as q, amount adsorbed at time t, versus t. The profiles were then predicted theoretically using two models: pseudo-first and

https://doi.org/10.1021/acsomega.3c01254
ACS Omega 2023, 8, 20697–20707

Table 1. Textural Properties of H, H350, and H500

adsorbent	activation conditions (t h, T °C)	BET surface area (m^2/g)	Langmuir surface area (m^2/g)	BJH pore volume (cm^3/g)	average pore size (nm)
H		0.5 ± 0.01	0.917 ± 0.040	0.00155 ± 0.00018	18.8
H350	2, 350	1.4 ± 0.06	2.160 ± 0.004	0.00181 ± 0.00057	26.8
H500	2, 500	16.9 ± 0.06	24.101 ± 0.583	0.14287 ± 0.00003	34.9

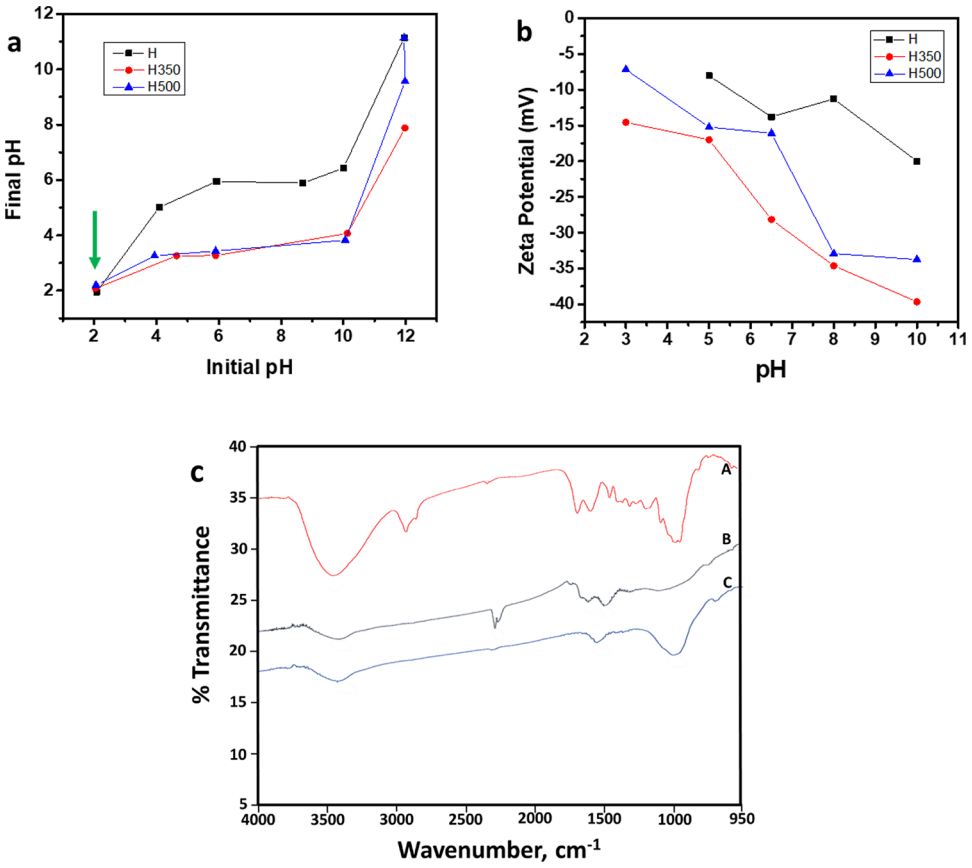

Figure 2. (a) PZC determination, (b) zeta potential of the three husks at different pH values, and (c) FT-IR spectra of H (A), H350 (B), and H500 (C). The green arrow in (a) points at the PZC where both initial and final pH values equate.

pseudo-second order models. The two respective models assume that the rate of uptake is directly proportional to the number and the square of the number of vacant sites. In the pseudo-second order model, adsorption is controlled by surface reaction, film and pore diffusion.[25] The integrated rate law equations pertaining to these models are given by eqs S3 and S4, respectively as shown in SI.[25−27]

2.4.4. Adsorption Isotherm Studies. The q_e vs C_e adsorption isotherms obtained from the previous experiments were fitted to different adsorption isotherm models; Langmuir, Freundlich, and linear isotherm models, as well as Dubinin−Radushkevich (D−R), and Temkin models.[18,28] The linear forms of these models are given in eqs S5, S6, S7, S8, S9, and S10, respectively as shown in the SI.[26,29,30] In the first model, a single monolayer of adsorbate is formed on a uniform adsorbent surface, with no interactions taking place between the adsorbate molecules. In the Freundlich model, however, not all the adsorption sites have the same energy; more energetically favorable sites are occupied first, and multilayer adsorption takes place. The linear adsorption model is the simplest isotherm model and assumed to be a special form of the Freundlich isotherm model where n = 1. The D−R was used to calculate the mean free energy of sorption and Temkin was used to estimate the heat of sorption.

2.5. Husk Regeneration. H350 was immersed for 3 h in a binary system containing 200 ppm of each of CA and SA. The husk was subsequently dried in an oven at 80 °C for 1 h and then immersed in 1 M HCl solution for 2 h. Finally, the husk was washed and dried again for 1 h at 80 °C. This process was repeated three more consecutive times.

2.6. Statistical Analysis. All measurements were performed in triplicate, and their respective means and standard deviations (expressed as mean ± SD) were determined accordingly. The two-tailed Student's t-test was used to examine the significant differences between results at a confidence level of 95%. Linear regression analysis was used to predict the equilibrium and kinetic profiles.

3. RESULTS AND DISCUSSION

3.1. Characteristics of the Husks. To analyze the morphology of the different husks, SEM was conducted and the images of H, H350, and H500 are shown in Figure 1a−c, respectively. Upon activation of the husk, its surface becomes smoother due to the chemical and thermal treatment which lead to dehydration, de-polymerization, and carbonization of

https://doi.org/10.1021/acsomega.3c01254
ACS Omega 2023, 8, 20697−20707

the husk. To determine the effect of activation on the surface area and pore volume of the husk, BET analysis was performed. The N_2 adsorption/desorption isotherms of H, H350, and H500 are depicted in Figure 1d−f, respectively. All husks exhibit Type IV isotherms with a small hysteresis loop, indicating a primarily mesoporous adsorbent which strongly interacts with the adsorbate. The hysteresis loop is Type 3, representing slit-shaped pores. The pore size distribution plots, shown in Figures S1 and S2, confirm the presence of a majority of mesopores ranging between 2 and 50 nm in size, along with some macropores which are larger than 50 nm. By comparing the BET and Langmuir surface areas as well as the pore volumes of the three husks (Table 1), it can be deduced that H500 followed by H350 have the largest BET and Langmuir surface area, as well as pore volume. The BET surface areas of H500 and H350 exceed that of H by about 34 and 3 times, respectively, whereas their pore volumes are 89 and 1.3 times higher than H, respectively. The activation, therefore, increases the surface area and pore volume of the husk, which, in turn, is anticipated to enhance its adsorption capacity. It is important to note, however, that the surface area and pore volume are not the sole factors which influence the adsorption capacity of the husk, since not all pores are necessarily active sites for adsorption.

The isoelectric pH or the PZC of the adsorbent is the pH at which the net surface charge of the adsorbent is equal to zero. PZC is important in understanding the mechanisms by which the contaminants are bound to the husk.[18] A plot of final pH of the solution vs its initial pH has thus been constructed (Figure 2a). The pH at which both equate is the PZC, which is 2.0 for all three husk preparations. This implies that the husk is positively charged at pH values lower than 2.0 and is negatively charged at pH values greater than 2.0.

To determine the charge on each husk, their respective zeta potentials (ZP) were measured at different pH values (Figure 2b). The zeta potential results are in accordance with the results obtained from the PZC measurements given above, i.e., for all three husks, the zeta potential is negative at pH > 2 and becomes more negative, as the solution pH increases. A zeta potential equal to or more negative than −30 mV typically indicates a stable colloid.[31] Clearly, H350 shows the most negative ZP, followed by H500, and then H. Thus, H350 is the most stable husk, and this is one of the reasons it was chosen as the optimal husk for conducting further studies.

The FT-IR spectra of the three investigated husks are analyzed to determine the main functional groups present on each husk (Table 2 and Figure 2c). All three types of husks show a band at 3434 cm^{-1} indicating the presence of a hydroxyl group or an N−H group, as has similarly been reported in Tomatillo husk which belongs to the same plant genus of cape gooseberries.[14] H shows a band at 1053 cm^{-1} which is possibly due to the stretching of the C−OH bond, which is weakened in H350 and shifted to 1093 cm^{-1} in H500 most likely due to husk activation. Another band appears in the spectrum of H at 2922 cm^{-1} which could be ascribed to the C−H stretch, also present in Tomatillo husk.[14] This band is not present in H350 and H500 most likely due to the carbonization and the activation of the husk. These previous changes can be attributed to the breakage of the C−OH and C−H bonds and loss of water after activation. In addition, the presence of a band at 1722−1732 cm^{-1} in the spectrum of H indicates the presence of a C═O, which gets weakened in the spectrum of H350 and disappears in the spectrum of H500 consistent with the carbonization and CO_2 release during the activation process. The bands at 1610−1650 cm^{-1} in the three husks correspond to either the C═C alkene stretch or the deformed bending vibrations of the adsorbed water molecules,[32−34] while the bands at 2300 cm^{-1} along with the bands at 650 cm^{-1} in H350 and H500 could be assigned to the adsorbed CO_2.[22] It can also be observed that the intensity of the CO_2 bands in the spectrum of H350 is higher than their counterparts in the H500 spectrum. The CO_2 could have been entrapped inside the pores of H350, but escaped with the higher temperature treatment at 500 °C. In addition, the N−O band appearing at 1513 cm^{-1} in H disappeared in H350 and H500 due to husk carbonization. In the spectrum of H, the bands at 1251 and at 1372 cm^{-1} could be ascribed to the ester sulfate groups and the S═O group of sulfates, respectively. These groups probably belong to the polysaccharides present in the husk. The presence of acidic polysaccharides can also be confirmed by the band shown in the H spectrum at 1053 cm^{-1}.[22,35] These bands disappeared in H350 and H500 due to the carbonization. Overall, the activated husks exhibit a smaller number of FTIR peaks relative to the unactivated husk since activation involves breaking down and carbonization of the husk material.

Table 2. Main Functional Groups Present in H, H350, and H500 as Retrieved from the IR Spectra

functional group	wavelength (cm^{-1})	H	H350	H500
ester sulfate group	1260-1258	✓		
polysaccharides	1088-1012	✓		
C-OH	1050-1300	✓	✓	✓
N-O	1500-1550	✓		
C=O	1670-1820	✓	✓	
C- H	2850-3000	✓		
O-H/N-H	3300-3500	✓	✓	✓

3.2. Parameters Affecting Biosorption. The effects of operating parameters (initial concentration and pH) on two biosorption indicators (q_e and removal percentage) are studied. The pH is one of the key parameters that affects the adsorption process since it affects the surface charge of the adsorbent as well as the degree of ionization of the adsorbate. The effect of pH on the adsorption of SA was investigated at an initial SA concentration of 70 mg/L and different pH values ranging from 2 to 12. Figure 3a,b shows the respective % removal and q_e of SA and CA onto H350 at different pH values. The corresponding data pertaining to H and H500 are shown in the same figure. For all husk preparations, particularly H and H500, both the removal and q_e of SA decrease with increasing the pH above 7. In the acidic region, no significant change, according to Student's *t*-test, can be observed in the removal or q_e of each husk with pH. The percent removal of SA in this region reaches up to 70% onto H500, exceeding the removal onto H and H350 by 20%. As the pH increases above the PZC of the husk (i.e., pH = 2) and the pK_a of SA (i.e., 2.79), both SA and the husk become negatively charged, yet significant removal took place. This implies that the interaction between SA and the husk is unlikely to be electrostatic. For CA, both the removal and q_e decreased with increasing the pH up to 10.4, the pK_a of CA. As the pH approaches 10.4, the CA becomes less positively charged and hence its electrostatic interaction with the negatively charged husk weakens. By

https://doi.org/10.1021/acsomega.3c01254
ACS Omega 2023, 8, 20697−20707

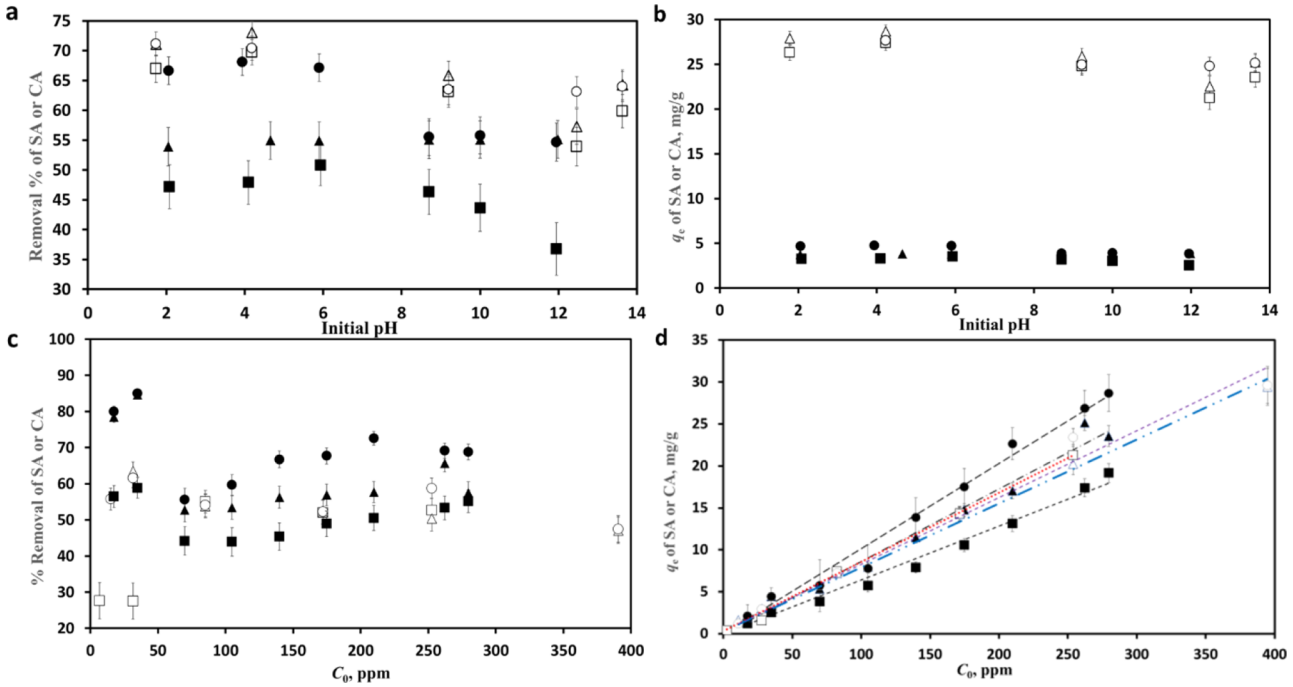

Figure 3. Effect of (a, b) pH and (c, d) initial concentration on the respective removal percentage and q_e of CA and SA on H, H350, and H500. In panels (a−d), all hollow markers represent data for CA, while solid markers represent data for SA. Triangles are for H350, squares for H, and circles for H500. Values are expressed as mean ± SD (n = 3). R^2 values for the regression lines shown in panel d range from 0.9781 to 0.9964.

Table 3. Kinetic Rate Constants (k_1 and k_2) for the Adsorption of SA (280 ppm) and CA (82 ppm) onto H, H350, and H500

contaminant	husk	k_1 (min^{-1})	R^2	RMSD	k_2 (g/mg min)	R^2	RMSD
SA	H	0.0035	0.5006	0.1053	0.7116	1.0000	0.0990
	H350	0.0009	0.6300	1.2786	0.4700	0.9999	0.6715
	H500	0.0014	0.4358	1.2492	0.1416	0.9998	1.2153
CA	H	0.0032	0.1063	0.2178	0.6775	0.9999	0.1301
	H350	0.0032	0.8493	0.1561	2.5959	1.0000	0.0642
	H500	0.0046	0.9451	0.1207	1.1909	1.0000	0.0503

generally comparing the adsorption performance of the three husks, it can be inferred that they all show comparable removal efficiencies at the same pH, as well as comparable adsorption capacities. In view of the above results, pH 6.5 is chosen as the working pH for the rest of the study since it provides the optimum percent removal for both SA and CA under almost neutral conditions which are favorable for operation.

The effect of initial concentration on the percentage removal of SA and CA by H350 is evaluated in the concentration range of 18−280 and 1.5−400 mg/L, respectively, at pH 6.5 ± 0.2 as depicted in Figure 3c. The corresponding profiles for H and H500 are represented in the same figure. At all employed concentrations, the activated husks H350 and H500 exhibited higher SA removal efficiencies than H. This could be attributed to their higher surface areas and pore volumes relative to H. At the low concentrations (up to about 35 mg/L), H350 and H500 removed SA by up to 85% exceeding that of H by 1.4 times. However, at higher concentrations, the percent removal dropped and remained almost constant at about an average of 65, 55, and 50% for H500, H350, and H, respectively, indicating that the active sites have been almost saturated. Thus, the activation of the husk enhanced the removal of SA. As for CA removal, the activated husks H350 and H500 exhibited higher removal efficiencies than the un-activated husk H mainly at the lower concentrations (up to 25 mg/L), after which all three husks showed comparable removal efficiencies (∼55%). At the employed pH, the husk is negatively charged, while CA (pK_a = 10.4) is positively charged. Thus, electrostatic interaction most likely occurs between CA and the husk. Other possible physical interactions could take place but are probably minor relative to the electrostatic interactions. On the other hand, for SA adsorption, binding takes place despite the like charges possibly due to physical interaction via H-bonding and van der Waals forces (i.e., dipole−dipole interaction and dispersion forces). Thus, it is expected that the CA-husk interaction, being electrostatic, would be more favorable and stronger than the SA-husk interaction.

Figure 3d shows the effect of initial concentration on the q_e of CA and SA, respectively, onto H350, while the figure shows the same effect for the other two husks. The q_e of all husks increases with increasing the initial concentration, as a result of the higher concentration gradient which increases the mass transfer driving force.[18] The adsorption capacity of SA was best on H500, followed by H350 and then H, while the three husks showed comparable CA adsorption capacities.

3.3. Biosorption Kinetics. To predict the kinetic profiles for the adsorption of SA and CA onto the three husks, the experimental profiles obtained earlier were fitted to the pseudo-first order and pseudo-second order kinetic models

https://doi.org/10.1021/acsomega.3c01254
ACS Omega 2023, 8, 20697−20707

as shown in Figure S3. The corresponding rate constants, k_1 and k_2, are listed in Table 3. The kinetic profiles are best described by the pseudo-second order kinetic model, for both SA and CA, as evident from the higher R^2 and the lower root mean standard deviation (RMSD) values relative to their pseudo-first order counterparts (Table 3, Figure S3). This is consistent with previous work dealing with the adsorption of SA and CA onto different other adsorbents.[2,11,36] By comparing the pseudo-second order kinetic rate constants, k_2, it can be deduced that the rate of adsorption of SA onto H350 is much higher (>3 times) than its rate of adsorption onto H500, possibly owing to the significantly larger pore volume and larger average pore size of H500 relative to H350, as previously confirmed by BET. As a result, the adsorption onto H500 is more likely governed by slow pore diffusion kinetics rather than fast surface reaction kinetics. Adsorption of SA onto H exhibited the highest rate since H has the smallest pore volume among the three husks and hence adsorption occurred mainly through instantaneous surface reaction. As for the rate of adsorption of CA onto H350, on the other hand, it exceeds the rate of CA adsorption onto H500 and H by about 1.4 and 4 times, respectively. This could be explained in view of the more negative surface charge of H350, relative to H and H500 (Figure 2b), given that the interaction is anticipated to be electrostatic.

3.4. Biosorption Isotherms. The equilibrium adsorption isotherms for the binding of SA onto the three husks are shown in Figure S4a. By fitting the isotherms to the linear model (Figure S4a and Table S1) and the Langmuir model (Figure S4b and Table S1), moderately high and very low R^2 values were obtained. However as depicted in Figure S5a, the equilibrium isotherms for the adsorption of SA onto all husks are best fitted to the Freundlich isotherm model since it yields the best fit as indicated by its R^2 values (Table 4) that are higher than those of Langmuir and the linear models. In addition, having $n > 1$ for these isotherms confirms the favorability of SA adsorption onto these husks. In particular, adsorption onto the activated husks is more favorable ($n > 1.2$) than that onto the un-activated husk ($n \sim 1$). The K_F constants for SA adsorption onto H350 and H500 (Table 4) are higher than their counterpart for H adsorption, which implies higher adsorption capacities onto the activated husks.

Table 4. Isotherm Parameters and Correlation Factors of the Freundlich Isotherm for SA and CA Adsorption onto the Three Husks

		K_F ($mg^{1-(1/n)}$ g^{-1} $L^{1/n}$)	n	R^2
SA	H	1.822	1.098	0.952
	H350	3.711	1.217	0.929
	H500	7.556	1.232	0.994
CA	H	0.287	1.124	0.998
	H350	0.414	1.257	0.998
	H500	0.375	1.224	0.999

Similarly, the isotherms pertaining to the adsorption of CA onto the three husks were fitted to the three models as presented in Figure S4c,d, Figure S5b, Tables 4 and S1, and showed the best fit to the Freundlich model. Fitting the data to the Langmuir model yielded very low R^2-values and/or negative slopes (Figure S4d, Table S1). The K_F constants for CA adsorption onto H350 and H500 (Table 4) are slightly higher than their counterpart for H adsorption (Table S1), which implies slightly higher adsorption capacities onto the activated husks. As with SA, adsorption onto the activated husks is more favorable, as implied from the n values, than that onto the un-activated one. Furthermore, the optimal husk H350 has higher favorability for CA than SA.

To gain more insight into the mechanism of sorption as to whether it is a chemical or physical one, the adsorption isotherms of SA and CA onto the three husks were fitted to the D−R model (Figure S6a and b).[28,37] The relevant adsorption energies are calculated using eqs S8 and S9[38,39] and are summarized in Table S2. The data obtained show all energies of adsorption to be below 8 kJ/mol, suggesting physisorption of SA and CA onto all three husks. Furthermore, the energies for the adsorption of CA onto the three husks are higher than their corresponding values for the adsorption of SA, in line with the findings obtained from the above biosorption studies which suggested that CA binds more strongly to the husk than SA.

The Temkin isotherm model (eq S10) was also investigated as shown in Figure S7a,b and Table S1 for the adsorption of both SA and CA on the three husks. The values of the B constant which are related to the heat of sorption are positive indicating an exothermic process.[40]

3.5. Proposed Removal Mechanism. Figure 4 shows that CA gets adsorbed onto the husk via electrostatic interaction, while SA is adsorbed via weaker physical interactions (e.g., H-bonding and van der Waals forces). The adsorption of CA onto the husk was sensitive to the working pH and decreased as the pH was approaching the pK_a of CA, i.e., when the CA charge was becoming less positive while the husk was negative. On the other hand, the SA adsorption was much less sensitive to the pH variation, and the SA was significantly removed, despite the like negative charges of both SA and the husk. Within the working pH range of 2−12, the hydroxyl and amine groups of the husk can H-bond with both SA and its carboxylate anion.[36] In the pH 4−12, the monoprotic anionic species of SA is dominant, while its neutral form is more prominent at pH < 4.

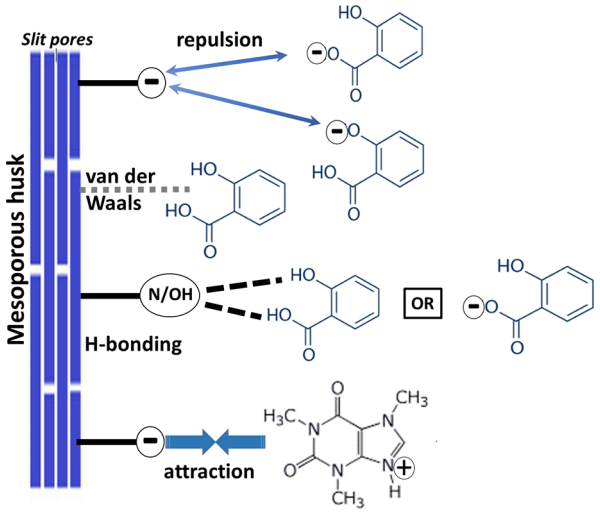

Figure 4. Proposed mechanism for the adsorption of SA and CA onto the husk.

Since electrostatic interactions are stronger than physical interactions, this resulted in a stronger CA-husk interaction, compared to that of SA-husk. This is consistent with the higher

https://doi.org/10.1021/acsomega.3c01254
ACS Omega 2023, 8, 20697−20707

CA adsorption energies onto the three husks relative to their SA counterparts. For the optimal H350 husk, it binds more favorably to CA than SA as indicated by its higher n constant, estimated by the Freundlich model, as well as the higher husk affinity and selectivity for CA over SA (as discussed in the binary study in the next section). The H350 husk had the highest zeta potential at the working pH, the highest negative charge and therefore the strongest electrostatic interaction with the positively charged CA, making it the most efficient husk in removing CA.

3.6. Binary Adsorption Studies and Husk Regeneration. The adsorption of SA and CA onto H350 is studied in binary systems, where both adsorbates are applied at equal initial concentrations. H350 is chosen for this study because of the following reasons: (i) the removal percentages of each of SA and CA onto H350 and H500 were very comparable and higher than H, (ii) H350 provided the highest adsorption rate for CA, and higher adsorption rate than H500 for both SA and CA; (iii) H350 has the highest colloidal stability which is desirable for efficient operation; and (iii) the preparation of H350 is less energy intensive. Figure 5 shows the simultaneous

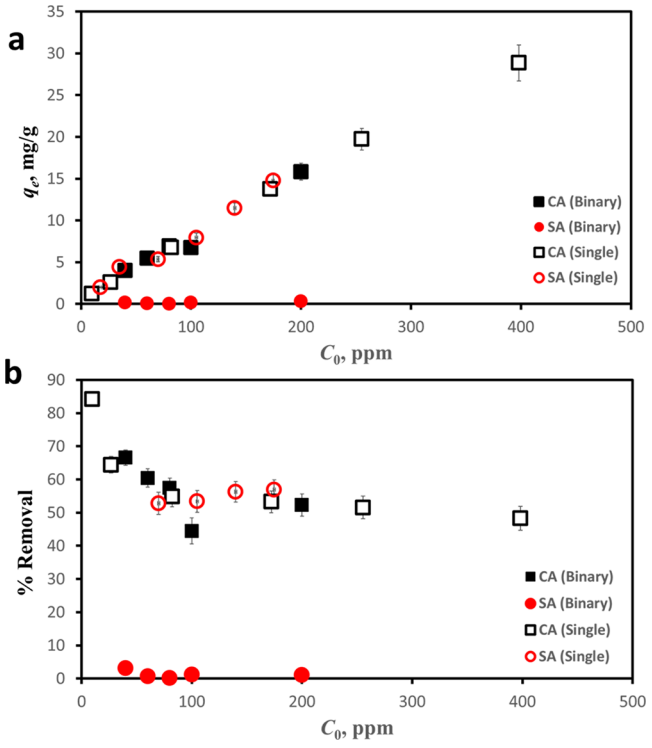

Figure 5. Adsorption capacity (a) and % removal (b) of CA and SA onto H350 in a binary system as a function of initial concentration. Confidence intervals are expressed as mean ± SD (n = 3).

adsorption of SA and CA onto H350 in a binary solution constituting the two contaminants at equal initial concentrations and in a ratio of 1:1. As shown, q_e of each of SA (solid circle) and CA (solid square) in the binary system is recorded at different initial concentrations (Figure 5a). The figure also shows the corresponding single component values for SA (hollow circle) and CA (hollow square). Clearly, q_e of CA, in both binary and single-component systems, increases with initial concentration, showing comparable capacities in both systems. Thus, the husk has much higher affinity for CA than for SA and hence is selective for CA. CA is highly competitive due to its ability to bind electrostatically to the husk, while SA adsorbs by only weak physical interactions. Similarly, % removal of SA and CA was plotted at different initial concentrations of the binary system (Figure 5b). The removal of CA in the binary system is comparable to its removal in the single system which confirms that it faced minimal competition from SA over the adsorption sites. On the other hand, the % removal and q_e of SA in the binary system are much lower than their counterparts in the single-component system, manifesting the effect of the competition from CA.

To quantify how selective the husk is to CA over SA, the selectivity coefficient, α, is calculated following eq S11,[41] for different initial concentrations, C_0. The different values of α as a function of C_0 are summarized in Table S3 and Figure S8. As the initial concentration doubles from 40 to 80 ppm, the selectivity coefficient of CA over SA sharply increases (about 10 times) from 60.8 to reach a peak at 627.3. At higher concentrations, the selectivity decreases once again to nearly its initial value and levels off. Despite the important variations in the values of α over the different initial concentrations, the values remain high in the whole concentration window, further demonstrating the favorable adsorption of CA onto the husk, compared to that of SA. In view of the above discussion, the water treatment system for CA and SA removal can be designed to encompass two stages, a first stage where CA is captured onto the husk and almost all SA remains in the solution, and a second stage that is fed by the SA effluent solution from the first stage. SA will thus be removed as a single component in the second stage.

The regenerability of the chosen husk (H350) was tested by immersing it in 1.0 M HCl solution for 2 h. Both SA and CA were first adsorbed then desorbed for four consecutive cycles. The adsorption capacity and percent removal were calculated after each cycle as given in Figure 6. The % removal of CA only decreased from 50.9 to 49.2% after 4 cycles, while SA was almost unremoved from the solution due to the competitive nature of CA. This suggests that the husk can be efficiently reused for up to four cycles, without significantly impacting its adsorption performance.

4. CONCLUSIONS

The agri-food waste cape gooseberry husk was, for the first time, utilized as a sorbent which successfully removed CA and SA from aqueous solutions. Three different preparations of unactivated and activated husks were characterized, demonstrating the importance of husk activation in increasing the surface area, pore volume, average pore size and adsorption favorability. Above 80 and 60% removal for SA and CA respectively in single systems was achieved under the investigated set of conditions; however, higher values could possibly be obtained by changing the adsorbent amount. Adsorption of SA and CA onto all husks followed the pseudo-second order kinetic model. H350 showed the highest maximal removal efficiencies of SA and CA, high rates of adsorption, and highest colloidal stability. In addition, this husk offered a less energy intensive option in its preparation than H500. Data on the characterization measurements, biosorption indicators, kinetic modeling, and isotherm models were presented, and a removal mechanism of CA and SA was proposed: CA interacts electrostatically with the husk, while SA binds through weak physical interactions. Accordingly, in the binary system, CA adsorption was highly favored over SA adsorption. Additionally, the husk was efficaciously regenerated and re-used for up

https://doi.org/10.1021/acsomega.3c01254
ACS Omega 2023, 8, 20697−20707

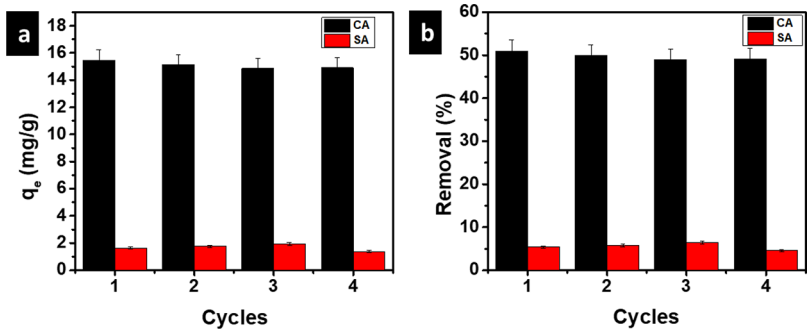

Figure 6. (a) Adsorbed quantity and (b) removal percentage of CA and SA onto H350 after husk regeneration for four cycles. Confidence intervals are expressed as mean ± SD (n = 3).

to four consecutive cycles, further manifesting the viability of utilizing activated cape gooseberry husk as an efficient eco-friendly biosorbent in water treatment. The novel use of cape gooseberry husk could be extended to other contaminants of emerging concern. In view of the high selectivity of the husk to CA, a two-stage separation system is proposed to sequentially remove CA in the first stage, followed by SA in the second stage.

■ ASSOCIATED CONTENT

Data Availability Statement

The datasets used and/or analyzed during the current study are available from the corresponding author on reasonable request.

Supporting Information

The Supporting Information is available free of charge at https://pubs.acs.org/doi/10.1021/acsomega.3c01254.

BJH pore size distribution for (a) H, (b) H350, and (c) H500; pore volume distribution per pore diameter; (a) pseudo-first order and (b) pseudo-second order kinetic plots for the adsorption of SA (280 ppm) onto H, H350, and H500, (c) pseudo-first order and (d) pseudo-second order kinetic plots for the adsorption of CA (82 ppm) onto H, H350, and H500; equilibrium adsorption isotherms of (a) SA and (c) CA onto H, H350, and H500, as fitted to the linear model; values are expressed as mean ± SD (n = 3); Langmuir isotherm linear plots for the adsorption of (b) SA and (d) CA onto H, H350 and H500; for all data, pH = 6.5 ± 0.2 and T = 27 °C ± 2; Freundlich isotherm linear plots for the adsorption of (a) SA and (b) CA onto H, H350 and H500; for all data, pH = 6.5 ± 0.2 and T = 27 °C ± 2; D−R isotherm model for the adsorption of (a) SA and (b) CA onto the three husks; Temkin isotherm model for the adsorption of (a) SA and (b) CA onto the three husks; selectivity coefficient of CA over SA in the binary system, at different initial concentrations; isotherm parameters and correlation factors for the linear, Langmuir, and Temkin isotherms for SA and CA adsorption onto the three husks; E (kJ/mol) values, as estimated from the D−R model, for the adsorption of SA and CA onto H, H350, and H500; and calculation of selectivity coefficients of CA over SA, at different initial concentrations, in the binary system (PDF)

■ AUTHOR INFORMATION

Corresponding Authors

Tamer Shoeib − *Department of Chemistry, School of Sciences and Engineering, The American University in Cairo, 11835 Cairo, Egypt;* orcid.org/0000-0003-3512-1593; Email: T.Shoeib@aucegypt.edu

Mayyada M. H. El-Sayed − *Department of Chemistry, School of Sciences and Engineering, The American University in Cairo, 11835 Cairo, Egypt;* orcid.org/0000-0001-6257-5748; Email: Mayyada@aucegypt.edu

Authors

Jehan Abdel Salam − *Department of Chemistry, School of Sciences and Engineering, The American University in Cairo, 11835 Cairo, Egypt*

Amina A. Saleh − *Department of Chemistry, School of Sciences and Engineering, The American University in Cairo, 11835 Cairo, Egypt;* orcid.org/0000-0003-0631-517X

Toqa Taha El Nenaiey − *Department of Chemistry, School of Sciences and Engineering, The American University in Cairo, 11835 Cairo, Egypt*

Hu Yang − *State Key Laboratory of Pollution Control and Resource Reuse, School of the Environment, Nanjing University, Nanjing 210023, P. R. China; Quanzhou Institute for Environmental Protection Industry, Nanjing University, Quanzhou 362000, P. R. China;* orcid.org/0000-0001-5779-1833

Complete contact information is available at: https://pubs.acs.org/10.1021/acsomega.3c01254

Author Contributions

‖J.A.S. and A.A.S. equally contributed to this work.

Funding

This work was supported by The American University in Cairo and by USAID ASHA grant number: AID-ASHA-G-17-00010. The work was also partially funded by a grant from the Egyptian Academy of Scientific Research and Technology in its Bilateral Program with the National Natural Science Foundation of China.

Notes

The authors declare no competing financial interest.

■ REFERENCES

(1) Gao, B.; Chang, Q.; Xi, Z.; El-Sayed, M. M. H.; Shoeib, T.; Yang, H. Fabrication of environmentally-friendly composited sponges for efficient removal of fluoroquinolones antibiotics from water. *J. Hazard. Mater.* **2022**, *426*, No. 127796.

(2) Álvarez, S.; Ribeiro, R. S.; Gomes, H. T.; Sotelo, J. L.; García, J. Synthesis of carbon xerogels and their application in adsorption studies of caffeine and diclofenac as emerging contaminants. *Chem. Eng. Res. Des.* **2015**, *95*, 229−238.
(3) Ayyash, F.; Kamis, M.; Khalaf, S.; Thawabteh, A.; Karaman, R. *Removal of Aspirin, Salicylic Acid, Paracetamol and p-Aminophenol by Advanced Membrane technology Activated Charcoal and Clay Micelles Complex*; Social Science Research Network: Rochester, NY, 2015. https://papers.ssrn.com/abstract=3402299 (accessed March 1, 2022).
(4) Mohamed, H. F.; Awad, B. M.; Abd El Rahman, S.; El-Sayed, M. M. H. Purification of Industrial Wastewater from Methylene Blue (MB) Dye Using Organic and Inorganic Sol−gel Glasses. *J. Sci. Res. Sci.* **2018**, *35*, 400−416.
(5) El-Sayed, M. M. H.; Elsayed, R. E.; Attia, A.; Farghal, H. H.; Azzam, R. A.; Madkour, T. M. Novel nanoporous membranes of bio-based cellulose acetate, poly(lactic acid) and biodegradable polyurethane in-situ impregnated with catalytic cobalt nanoparticles for the removal of Methylene Blue and Congo Red dyes from wastewater. *Carbohydr. Polym. Technol. Appl.* **2021**, *2*, No. 100123.
(6) de Oliveira, M.; Atalla, A. A.; Frihling, B. E. F.; Cavalheri, P. S.; Migliolo, L.; Filho, F. J. C. M. Ibuprofen and caffeine removal in vertical flow and free-floating macrophyte constructed wetlands with Heliconia rostrata and Eichornia crassipes. *Chem. Eng. J.* **2019**, *373*, 458−467.
(7) Richardson, S. D.; Kimura, S. Y. Water Analysis: Emerging Contaminants and Current Issues. *Anal. Chem.* **2016**, *88*, 546−582.
(8) Pathak, P. D.; Mandavgane, S. A.; Kulkarni, B. D. Utilization of banana peel for the removal of benzoic and salicylic acid from aqueous solutions and its potential reuse. *Desalin. Water Treat.* **2016**, *57*, 12717−12729.
(9) Arshadi, M.; Mousavinia, F.; Abdolmaleki, M. K.; Amiri, M. J.; Khalafi-Nezhad, A. Removal of salicylic acid as an emerging contaminant by a polar nano-dendritic adsorbent from aqueous media. *J. Colloid Interface Sci.* **2017**, *493*, 138−149.
(10) Smiljanić, D.; Daković, A.; Obradović, M.; Ožegović, M.; Izzo, F.; Germinario, C.; de Gennaro, B. Application of Surfactant Modified Natural Zeolites for the Removal of Salicylic Acid—A Contaminant of Emerging Concern. *Materials* **2021**, *14*, 7728.
(11) Fu, Z.; Li, H.; Yang, L.; Yuan, H.; Jiao, Z.; Chen, L.; Huang, J.; Liu, Y.-N. Magnetic polar post-cross-linked resin and its adsorption towards salicylic acid from aqueous solution. *Chem. Eng. J.* **2015**, *273*, 240−246.
(12) Lee, X. J.; Chemmangattuvalappil, N.; Lee, L. Y. Adsorptive Removal of Salicylic Acid from Aqueous Solutions using New Graphene-Based Nanosorbents. *Chem. Eng. Trans.* **2015**, *45*, 1387−1392.
(13) Sotelo, J. L.; Ovejero, G.; Rodríguez, A.; Álvarez, S.; Galán, J.; García, J. Competitive adsorption studies of caffeine and diclofenac aqueous solutions by activated carbon. *Chem. Eng. J.* **2014**, *240*, 443−453.
(14) García-Mendieta, A.; Olguín, M. T.; Solache-Ríos, M. Biosorption properties of green tomato husk (Physalis philadelphica Lam) for iron, manganese and iron−manganese from aqueous systems. *Desalination* **2012**, *284*, 167−174.
(15) Mallek, M.; Chtourou, M.; Portillo, M.; Monclús, H.; Walha, K. Granulated cork as biosorbent for the removal of phenol derivatives and emerging contaminants. *J. Environ. Manage.* **2018**, *223*, 576−585.
(16) El-Sayed, H. E. M.; El-Sayed, M. M. H. Assessment of Food Processing and Pharmaceutical Industrial Wastes as Potential Biosorbents: A Review. *BioMed Re. Int.* **2014**, *2014*, No. e146769.
(17) Bădescu, I. S.; Bulgariu, D.; Ahmad, I.; Bulgariu, L. Valorisation possibilities of exhausted biosorbents loaded with metal ions − A review. *J. Environ. Manage.* **2018**, *224*, 288−297.
(18) Bayomie, O. S.; Kandeel, H.; Shoeib, T.; Yang, H.; Youssef, N.; El-Sayed, M. M. H. Novel approach for effective removal of methylene blue dye from water using fava bean peel waste. *Sci. Rep.* **2020**, *10*, 7824.
(19) Mohammad, S. G.; El-Sayed, M. M. H. Removal of imidacloprid pesticide using nanoporous activated carbons produced via pyrolysis of peach stone agricultural wastes. *Chem. Eng. Commun.* **2021**, *208*, 1069−1080.
(20) Ali, A.; Singh, B. P. Studies on production potential of cape gooseberry (Physalis peruviana L.) in sodic soil under varying agronomic manipulations, Journal of Applied and Natural. *Science* **2016**, *8*, 368−374.
(21) Ahmed, L. A. Renoprotective Effect of Egyptian Cape Gooseberry Fruit (Physalis peruviana L.) against Acute Renal Injury in Rats. *Sci. World J.* **2014**, *2014*, No. e273870.
(22) Essa, H. L.; Guirguis, H. A.; El-Sayed, M. M. H.; Rifaat, D.; Abdelfattah, M. S. Ultrasonically-Extracted Marine Polysaccharides as Potential Green Antioxidant Alternatives. *Proceedings* **2020**, *67*, 23.
(23) Sorour, M. H.; Hani, H. A.; Shaalan, H. F.; El Sayed, M. M.; El-Sayed, M. M. H. Softening of seawater and desalination brines using grafted polysaccharide hydrogels. *Desalin. Water Treat.* **2015**, *55*, 2389−2397.
(24) Gao, B.; Tao, K.; Xi, Z.; El-Sayed, M. M. H.; Shoeib, T.; Yang, H. Fabrication of 3D lignosulfonate composited sponges impregnated by BiVO4/polyaniline/Ag ternary photocatalyst for synergistic adsorption-photodegradation of fluoroquinolones in water. *Chem. Eng. J.* **2022**, *446*, No. 137282.
(25) Morcos, G. S.; Ibrahim, A. A.; El-Sayed, M. M. H.; El-Shall, M. S. High performance functionalized UiO metal organic frameworks for the efficient and selective adsorption of Pb (II) ions in concentrated multi-ion systems. *J. Environ. Chem. Eng.* **2021**, *9*, No. 105191.
(26) Zafar, L.; Khan, A.; Kamran, U.; Park, S.-J.; Bhatti, H. N. Eucalyptus (camaldulensis) bark-based composites for efficient Basic Blue 41 dye biosorption from aqueous stream: Kinetics, isothermal, and thermodynamic studies. *Surf. Interfaces* **2022**, *31*, No. 101897.
(27) Samimi, M.; Shahriari-Moghadam, M. Isolation and identification of Delftia lacustris Strain-MS3 as a novel and efficient adsorbent for lead biosorption: Kinetics and thermodynamic studies, optimization of operating variables. *Biochem. Eng. J.* **2021**, *173*, No. 108091.
(28) Mostafapour, F. K.; Yilmaz, M.; Mahvi, A. H.; Younesi, A.; Ganji, F.; Balarak, D. Adsorptive removal of tetracycline from aqueous solution by surfactant-modified zeolite: equilibrium, kinetics and thermodynamics, Desalination. *Water Treat.* **2022**, *247*, 216−228.
(29) Langmuir, I. The Adsorption Of Gases On Plane Surfaces Of Glass, Mica And Platinum. *J. Am. Chem. Soc.* **1918**, *40*, 1361−1403.
(30) Sorour, M. H.; Hani, H. A.; Shaalan, H. F.; El-Sayed, M. M. H. Experimental screening of some chelating agents for calcium and magnesium removal from saline solutions. *Desalin. Water Treat.* **2016**, *57*, 22799−22808.
(31) Honary, S.; Zahir, F. Effect of Zeta Potential on the Properties of Nano-Drug Delivery Systems - A Review (Part 1). *Trop. J. Pharm. Res.* **2013**, *12*, 255−264.
(32) Jozanikohan, G.; Abarghooei, M. N. The Fourier transform infrared spectroscopy (FTIR) analysis for the clay mineralogy studies in a clastic reservoir. *J. Pet. Explor. Prod. Technol.* **2022**, *12*, 2093−2106.
(33) Selimin, M. A.; Latif, A. F. A.; Er, Y. C.; Muhamad, M. S.; Basri, H.; Lee, T. C. Adsorption efficiency of banana blossom peels (musa acuminata colla) adsorbent for chromium (VI) removal. *Mater. Today Proc.* **2022**, *57*, 1262−1268.
(34) Zhao, F.; Shan, R.; Li, W.; Zhang, Y.; Yuan, H.; Chen, Y. Synthesis, Characterization, and Dye Removal of ZnCl2-Modified Biochar Derived from Pulp and Paper Sludge. *ACS Omega* **2021**, *6*, 34712−34723.
(35) Abou El Azm, N.; Fleita, D.; Rifaat, D.; Mpingirika, E. Z.; Amleh, A.; El-Sayed, M. M. H. Production of Bioactive Compounds from the Sulfated Polysaccharides Extracts of Ulva lactuca: Post-Extraction Enzymatic Hydrolysis Followed by Ion-Exchange Chromatographic Fractionation. *Molecules* **2019**, *24*, 2132.
(36) Essandoh, M.; Kunwar, B.; Pittman, C. U.; Mohan, D.; Mlsna, T. Sorptive removal of salicylic acid and ibuprofen from aqueous

https://doi.org/10.1021/acsomega.3c01254
ACS Omega 2023, 8, 20697−20707

solutions using pine wood fast pyrolysis biochar. *Chem. Eng. J.* **2015**, *265*, 219−227.
(37) Inyinbor, A. A.; Adekola, F. A.; Olatunji, G. A. Kinetics, isotherms and thermodynamic modeling of liquid phase adsorption of Rhodamine B dye onto Raphia hookerie fruit epicarp. *Water Resour. Ind.* **2016**, *15*, 14−27.
(38) Liu, L.; Luo, X.-B.; Ding, L.; Luo, S.-L., Application of Nanotechnology in the Removal of Heavy Metal From Water. In *Nanomaterials for the Removal of Pollutants and Resource Reutilization*; Luo, X., Deng, F., Eds.; Elsevier, 2019; pp 83−147.
(39) Zhou, Y.; Li, Y.; Liu, D.; Liu, D.; Xu, L.; Liu, C. Adsorption optimization of uranium(VI) onto polydopamine and sodium titanate co-functionalized MWCNTs using response surface methodology and a modeling approach. *Colloids Surf., A* **2021**, *627*, No. 127145.
(40) Balarak, D.; Zafariyan, M.; Igwegbe, C. A.; Onyechi, K. K.; Ighalo, J. O. Adsorption of Acid Blue 92 Dye from Aqueous Solutions by Single-Walled Carbon Nanotubes: Isothermal, Kinetic, and Thermodynamic Studies. *Environ. Processes* **2021**, *8*, 869−888.
(41) Li, K.; Li, P.; Cai, J.; Xiao, S.; Yang, H.; Li, A. Efficient adsorption of both methyl orange and chromium from their aqueous mixtures using a quaternary ammonium salt modified chitosan magnetic composite adsorbent. *Chemosphere* **2016**, *154*, 310−318.

https://doi.org/10.1021/acsomega.3c01254
ACS Omega 2023, 8, 20697−20707